On-Surface Ullmann Coupling: The Influence of Kinetic Reaction Parameters on the Morphology and Quality of Covalent Networks

Johanna Eichhorn,[†,‡,§] Damian Nieckarz,[#] Oliver Ochs,[†,‡,∥] Debabrata Samanta,[⊥] Michael Schmittel,[⊥] Pawel Jerzy Szabelski,[#] and Markus Lackinger[†,‡,∥,*]

[†]Department of Physics, Technische Universität München, James-Franck-Str. 1, 85748 Garching, Germany, [‡]Center for NanoScience (CeNS), Schellingstr. 4, 80799 Munich, Germany, [§]TUM School of Education, Technische Universität München, Marsstraße 12, 80335 Munich, Germany, [⊥]Center of Micro- and Nanochemistry and Engineering, Organische Chemie I, Universität Siegen, Adolf-Reichwein-Str. 2, 57068 Siegen, Germany, [∥]Deutsches Museum, Museumsinsel 1, 80538 Munich, Germany, and [#]Department of Theoretical Chemistry, Maria Curie-Skłodowska University, Pl. M.C. Skłodowskiej 3, 20-031 Lublin, Poland

ABSTRACT On-surface Ullmann coupling is a versatile and appropriate approach for the bottom-up fabrication of covalent organic nanostructures. In two-dimensional networks, however, the kinetically controlled and irreversible coupling leads to high defect densities and a lack of long-range order. To derive general guidelines for optimizing reaction parameters, the structural quality of 2D porous covalent networks was evaluated for different preparation protocols. For this purpose, polymerization of an iodine- and bromine-functionalized precursor was studied on Au(111) by scanning tunneling microscopy under ultrahigh vacuum conditions. By taking advantage of the vastly different temperature thresholds for C—Br and C—I cleavage, two different polymerization routes were compared — hierarchical and direct polymerization. The structural quality of the covalent networks was evaluated for different reaction parameters, such as surface temperatures, heating rates, and deposition rates by statistical analysis of STM data. Experimental results are compared to Monte Carlo simulations.

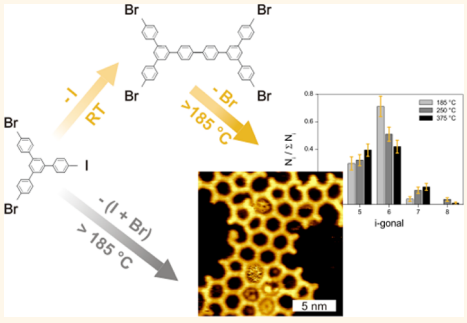

KEYWORDS: surface chemistry · polymerization · Au(111) · Ullmann coupling · scanning tunneling microscopy · Monte Carlo

Low-dimensional covalent organic nanostructures are promising novel functional materials for nanotechnological applications,[1,2] as they combine unprecedented chemical and mechanical stability with the vast tunability of organic materials. Their adjustable electronic band gap renders these materials highly interesting for applications in (opto)electronic devices.[3−5]

On-surface polymerization has become an established route for the tailored fabrication of covalent nanostructures. In recent years, various coupling reactions were applied for the fabrication of 1D and 2D covalent nanostructures including condensation reactions,[6,7] homocouplings of terminal alkynes (Glaser−Hay coupling),[8−10] and Ullmann coupling.[11−13] In the first step of the Ullmann coupling, brominated[14−16] or iodinated[11,17,18] precursors are deposited onto metal surfaces, typically under ultrahigh vacuum (UHV) conditions, even though this was also demonstrated under ambient conditions.[19,20] The weakly bound halogens are split off either directly upon adsorption or after additional thermal activation, and the resulting surface-stabilized radicals form kinetically inert C—C cross-links. Two-fold halogenated monomers yield virtually defect-free 1D structures, such as poly(3,4-ethylenedioxythiophene) chains,[21] poly(*para*-phenylene),[22] and graphene nanoribbons.[15] Similarly, 2D networks can be obtained with multiply halogenated monomers, yet with significantly lower structural quality, that is, high defect densities and rather small domain sizes.[23,24] The kinetic irreversibility of the newly formed C—C bonds impairs error correction.

The Ullmann coupling relies on the catalytic properties of the metal surface to activate the polymerization by splitting off the halogens. Accordingly, the surface plays an

* Address correspondence to markus@lackinger.org.

Received for review March 20, 2014 and accepted July 18, 2014.

Published online July 18, 2014
10.1021/nn501567p

active chemical role, and different influences arise in dependence on the metal. At room temperature, C−I bonds are spontaneously cleaved on Cu, Ag, and Au.[11,17] Bromine, instead, is fully split off on copper,[14,23] only partially on silver,[25,26] but not at all on gold, where additional thermal activation becomes necessary.[16] Density functional theory (DFT) simulations suggest that the energy barriers are around 0.3 eV smaller for deiodination than for debromination on Au(111), Ag(111), and Cu(111).[27] Subsequent to carbon−halogen cleavage, organometallic networks based on carbon−metal bonds were observed; 1D organometallic chains are ordered,[22,28] whereas 2D networks on copper remain disordered[14,23,25] but can be partially ordered on silver.[26,29] Even structural reorganization and equilibration of silver-based organometallic networks were demonstrated on Ag(111), indicating the reversibility of C−Ag bonds.[26] On gold, organometallic networks are less common but were occasionally observed.[30] A further important substrate influence arises from the surface mobility of the surface-stabilized radicals, as exemplified in a combined STM and Monte Carlo (MC) study of cyclohexa-*m*-phenylene (CHP), where improved networks were observed for an increasing ratio of diffusion to coupling.[17]

While the surface dependence of the Ullmann coupling has been thoroughly studied, the influence of controllable reaction parameters on the quality of 2D covalent networks remains largely unexplored. The present work tackles this open question by studying the polymerization of 1,3-bis(*p*-bromophenyl)-5-(*p*-iodophenyl)benzene (BIB, cf. Figure 1a) on Au(111). The unsymmetrical substitution with bromine and iodine as well as the particular choice of Au(111) facilitates comparative studies of direct *versus* hierarchical polymerization. Direct polymerization is realized by deposition onto a preheated surface, whereby both iodine and bromine are split off in the same polymerization step. Hierarchical polymerization is achieved by room temperature deposition, whereby iodine is selectively split off, whereas bromine remains stably bound. Only further thermal annealing also activates C−Br cleavage and thereby the full polymerization. This principle was already exploited by Grill and Hecht *et al*. using *trans*-Br_2I_2 tetraphenyl porphyrin.[31]

In the present work, influences of various reaction parameters on the morphology and quality of covalent networks were studied: for direct polymerization, the surface temperature during deposition and the deposition rate were varied, while for hierarchical polymerization, the heating rate and final surface temperature were investigated. The network quality was evaluated and quantified by statistical analysis of STM data. For enhanced insights, the experiments were accompanied by MC simulations.

RESULTS

Hierarchical Polymerization. Samples were prepared by deposition of BIB onto Au(111) at room temperature

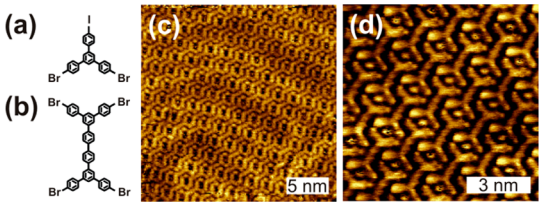

Figure 1. Chemical structures of BIB (a) and TBQ (b). Overview (−0.17 V, 35 pA) (c) and close-up STM images (+0.36 V, 3.5 pA) (d) of self-assembled TBQ structures acquired after room temperature deposition of BIB onto Au(111).

and subsequent thermal annealing. Prior to annealing, STM revealed self-assembly of dumbbell-shaped basic units (Figure 1). The herringbone reconstruction of Au(111) is still discernible (Figure 1c), indicating weak adsorbate−substrate interaction. The unit cell measures $a = (1.60 \pm 0.10)$ nm, $b = (1.64 \pm 0.10)$ nm, and $\gamma = 94.5 \pm 4.0°$ and contains one dumbbell with additional dots at its corners. The dumbbells appear with uniform height, that is, without internal STM contrast. For room temperature deposition, we anticipate the surface-assisted formation of BIB monoradicals through C−I cleavage followed by direct covalent cross-linking to dimers, that is 3,3‴,5,5‴-tetra(*p*-bromophenyl)-1,1′:4′,1″:4″,1‴-quaterphenyl (TBQ, cf. Figure 1b). Hence, the dots in the STM images can be assigned to surface-bound iodine. The coupling of two BIB to one TBQ releases two iodine atoms, whereas the self-assembled structure features only one iodine per TBQ. Yet, excess iodine was observed on terraces. In perfect agreement with STM, DFT gas phase geometry optimization of the dimer results in a length of 1.3 nm for the quaterphenyl backbone (cf. Supporting Information). The formation of metastable organometallic complexes, as typically observed on copper and silver,[14,25,29] would elongate the backbone to ∼1.6 nm in contradiction to the experiment. Interestingly, self-assembled dimers were similarly reported for fully brominated 1,3,5-tris-(*p*-bromophenyl)benzene (TBB) on Au(111) after heating to 110 °C.[16] Yet, in this case, the coexistence of dimers (TBQ), disordered structures, and unreacted monomers indicates an incomplete reaction. Furthermore, drop-casting of TBB under ambient conditions onto preheated Au(111) at 200 °C results in self-assembled TBQ monolayers with similar lattice parameters.[20]

The full polymerization of *in situ* synthesized TBQ was activated by subsequent thermal annealing. The required temperature for C−Br bond cleavage on Au(111) is around 175 °C (cf. Supporting Information), and after annealing to 185 °C, no unreacted TBQ was observed anymore. The covalent nature of the networks is unambiguously verified by an experimental center-to-center distance of interconnected monomers of 1.3 nm.

For hierarchical polymerization, the influences of both surface temperature and heating rate were studied by (1) heating samples with comparable rates of

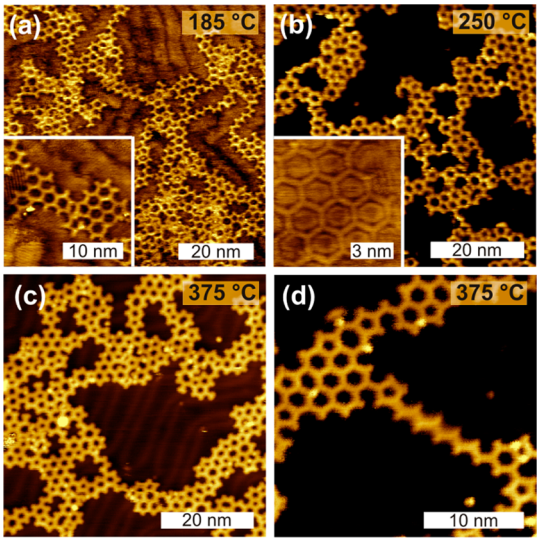

Figure 2. STM images of covalent networks prepared by room temperature deposition of BIB and subsequent thermal annealing (cf. Supporting Information for tunneling parameters). Due to preceding dimerization at room temperature, the actual monomer for the polymerization is the dumbbell-shaped TBQ. Thermal annealing was performed at different final temperatures of 185 °C (a), 250 °C (b), and 375 °C (c,d) as also indicated in the top right corners. All samples were annealed with comparable heating rates of 6.3 °C min^{-1} (a) or 8.9 °C min^{-1} (b–d).

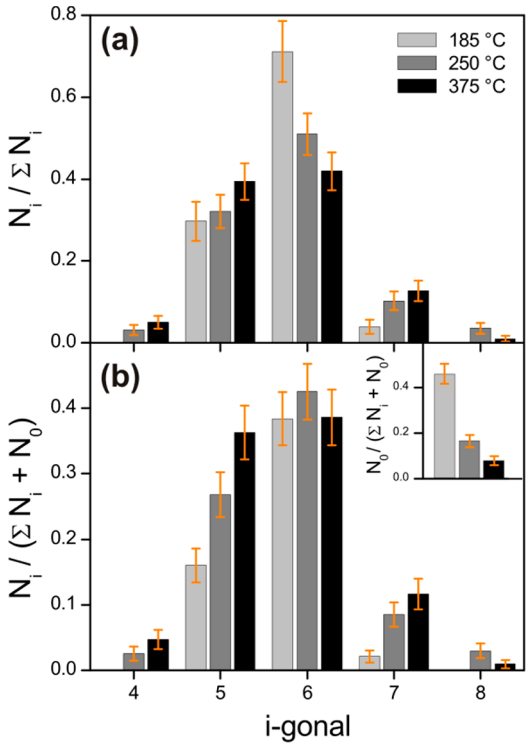

Figure 3. Pore geometry distributions of covalent networks prepared by hierarchical polymerization *via* room temperature deposition and subsequent annealing at different final temperatures (185, 250, and 375 °C) with similar heating rates of 6.3 or 8.9 °C min^{-1}. N_i and N_0 correspond to the number of *i*-gonal and open pores, respectively. Accordingly, the probabilities of *i*-gonal pores in (a) are referred to the total number of closed pores (ΣN_i), whereas in (b), N_i is normalized to the sum of closed and open pores ($\Sigma N_i + N_0$). The inset in (b) shows the relative amounts of open pores N_0 for the different final temperatures.

6.3–8.9 °C min^{-1} to 185, 250, and 375 °C (Figure 2), and (2) heating with variable rates of <0.1, 1.4, and 8.9 °C min^{-1} to a constant final temperature of 250 °C (Figure 4). The initial coverages for all experiments were comparable, and the samples were held at the final temperature for 15 or 70 min. Irrespective of the exact thermal treatment, all covalent networks were highly branched and composed of relatively small domains connected by filamentous structures of one-pore-wide strings or molecular chains (Figures 2 and 4). Besides the ideal hexagonal pores, irregular pores – tetragonal, pentagonal, heptagonal, and octagonal – were frequently observed. To quantify the structural quality of the networks, STM data were statistically analyzed (cf. Materials and Methods).

The corresponding pore geometry distributions of tetragonal to octagonal pores obtained for different final temperatures are depicted in Figure 3a. The counts were normalized to the total number of closed pores ΣN_i, with N_i corresponding to the counts of *i*-gonal pores. The highest probability for hexagonal pores was found for 185 °C. All covalent networks feature significant amounts of pentagonal pores as well as lower amounts of heptagonal pores. Tetragonal and octagonal pores are less frequently observed and were fully absent for 185 °C. Especially at lower polymerization temperatures, the network quality is significantly impaired by open, that is, incomplete pores (cf. inset Figure 3b). This is considered in the histogram in Figure 3b by renormalization of N_i to the sum of closed and open pores ($\Sigma N_i + N_0$). Direct comparison of both histograms indicates significant changes for polymerization at 185 °C, whereas the 250 and 375 °C distributions remain largely unaffected. In conclusion, the probability for irregular pores increases slightly with higher final temperatures, whereas polymerization at 185 °C results in a substantial amount of open pores.

Besides the final substrate temperature, also the influence of the heating rate on the network quality was investigated. STM images of the resulting structures are summarized in Figure 4. The statistical analysis for all heating rates yields almost identical pore geometry distributions (cf. Supporting Information), suggesting no decisive influence on the network quality.

Pore geometry distributions do not cover important structural aspects as the degree of compactness and the domain size. Respective structural information is contained in the pore coordination number, that is, the number of next nearest neighbors of a closed pore, whereby only closed pores were considered. Hence, the average pore coordination number (APCN) is introduced as a further statistical indicator of the network quality. In a perfect hexagonal network, the APCN

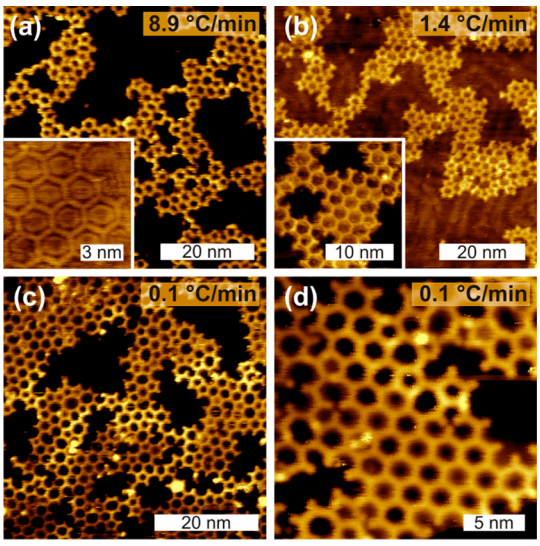

Figure 4. STM images of covalent networks prepared by room temperature deposition of BIB and subsequent thermal annealing (cf. Supporting Information for tunneling parameters). All samples were annealed at 250 °C, whereas different heating rates of 8.9 °C min^{-1} (a), 1.4 °C min^{-1} (b), and 0.1 °C min^{-1} (c,d) were applied. The insets depict close-up STM images of the most regular sample areas.

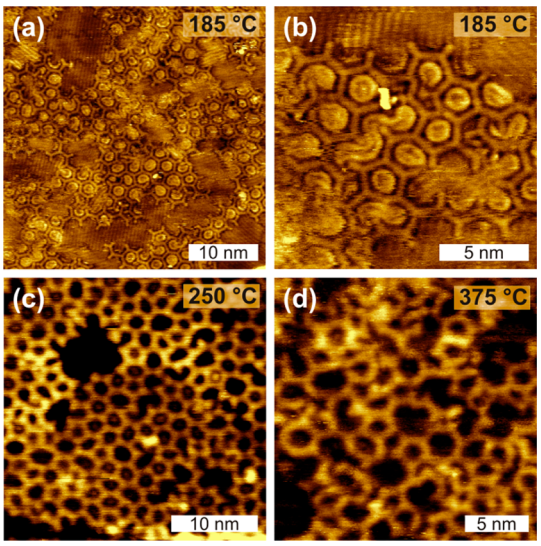

Figure 5. STM images of covalent networks prepared by deposition of BIB onto Au(111) held at 185 °C (a,b), 250 °C (c), and 375 °C (d) (cf. Supporting Information for tunneling parameters). The deposition rate corresponded to ~1.3 Hz s^{-1} for all experiments. After deposition, the samples were kept at the respective temperature for ~15 min.

is 6, whereas low values indicate the formation of branched networks. APCNs were evaluated for the different reaction parameters, and the underlying PCN distributions are summarized in the Supporting Information. For polymerization at 185 °C, an APCN of 1.9 is found, which is even below the value of 2.0 for infinite 1D pore chains. For enhanced surface temperatures of 250 and 375 °C, the APCNs increase to 3.0. Nevertheless, these comparatively low values underpin the branched and rugged nature of the covalent networks as already discernible in the STM images.

Direct Polymerization. In further experiments, direct polymerization was studied by depositing BIB onto preheated Au(111) at temperatures above the debromination threshold. Upon adsorption, both iodine and bromine substituents are readily split off, resulting in surface-stabilized triradicals that subsequently undergo polymerization. Yet, also for high-temperature deposition, a sequential polymerization with preceding dimerization can not *a priori* be excluded because both debromination and deiodination rates become enhanced. Hence, we postulate that the dissociation of both bromine and iodine is completed before coupling; that is, triradicals are the relevant species in direct polymerization. This hypothesis is supported by an experimental comparison of BIB *versus* TBB (the fully brominated analogue) polymerization. Statistical analysis of networks obtained by deposition of either monomer onto Au(111) held at 250 °C yield similar pore geometry distributions within experimental error (cf. Supporting Information).

For direct polymerization, the influences of surface temperature and deposition rate were independently studied in two series of experiments. The eigenfrequency decline $\Delta f/\Delta t$ of a quartz crystal microbalance (QCMB) serves as a quantitative measure of the deposition rate, whereby 1 Hz s^{-1} corresponds to about 0.1 monolayer min^{-1}.

The temperature influence was studied by depositing BIB with a constant rate onto preheated Au(111) held at 185, 250, and 375 °C. As already evident from the STM images in Figure 5, polymerization at either lower (185 °C) or higher (375 °C) temperature results in lower quality networks as compared to an intermediate temperature of 250 °C. The corresponding pore geometry distributions in Figure 6a reveal clear trends: The probability of pentagonal pores increases markedly with increasing substrate temperature, whereas the probability of regular hexagonal pores decreases. Similar to hierarchical polymerization, this behavior changes when the probabilities are renormalized to $\Sigma N_i + N_0$ (Figure 6b), especially for low-temperature polymerization. The high amount of open pores obtained for 185 °C significantly reduces the probability of hexagonal pores. For 250 and 375 °C, instead, the renormalization causes only minor changes. Evaluation of the APCN yields a very low value of 1.1 for 185 °C, which can be attributed to the high number of open pores. Surface temperatures of 250 and 375 °C result in increased APCNs of 4.3 and 2.6, respectively.

The influence of deposition rate in direct polymerization was studied by a further set of experiments where the deposition rates were varied over 2 orders of magnitude from <0.01 to 1.3 Hz s^{-1}. The surface temperature was kept constant at 250 °C. In order to exclude an additional influence of surface coverage, the deposition times were adjusted to yield comparable coverages.

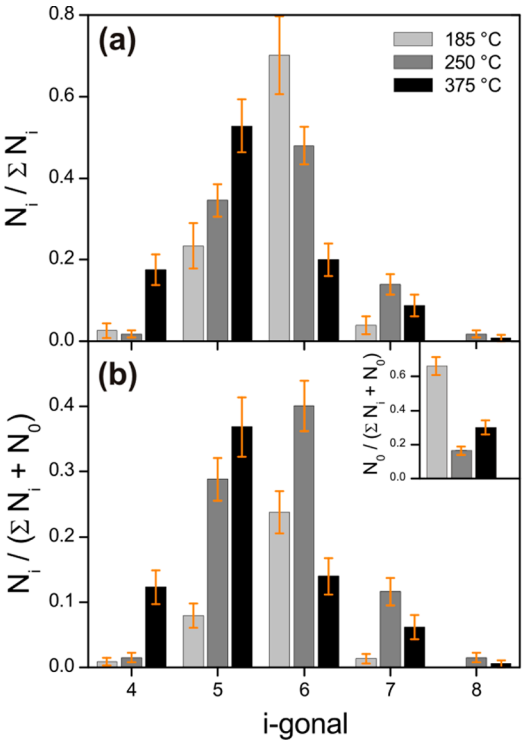

Figure 6. Pore geometry distributions of covalent networks prepared by direct polymerization *via* high-temperature deposition at 185, 250, and 375 °C. In all experiments, the deposition rates corresponded to ~1.3 Hz s^{-1}. N_i and N_0 have similar meaning as in Figure 3; that is, the probabilities of *i*-gonal pores in (a) are referred to ΣN_i, whereas in (b), N_i is normalized to $\Sigma N_i + N_0$. The inset in (b) shows N_0 for the different temperatures.

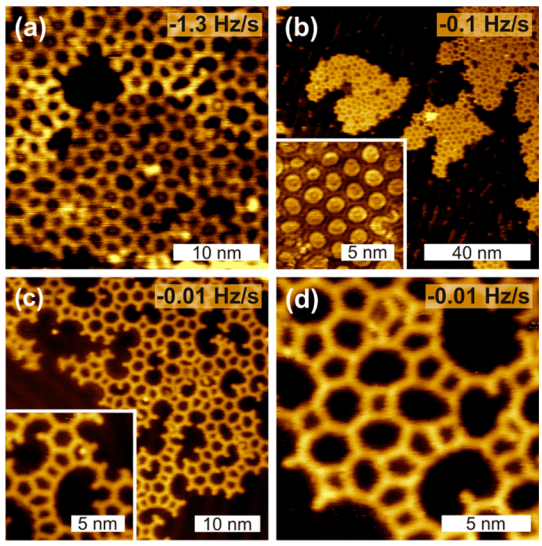

Figure 7. STM images of covalent networks prepared by deposition of BIB with varying rates corresponding to 1.3 Hz s^{-1} (a), 0.1 Hz s^{-1} (b), and 0.01 Hz s^{-1} (c,d) (cf. Supporting Information for tunneling parameters). In each experiment, the surface was held at a constant temperature of 250 °C.

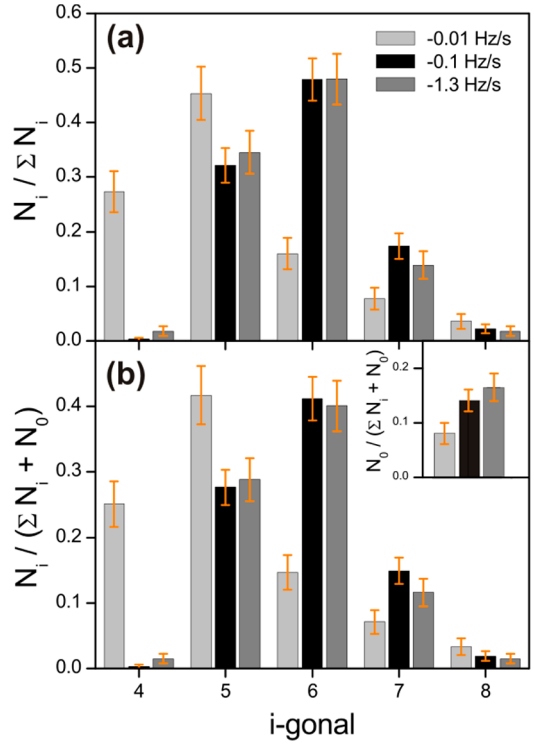

Figure 8. Pore geometry distributions of covalent networks formed by direct polymerization *via* high-temperature deposition at 250 °C. Different deposition rates corresponding to 0.01, 0.10, and 1.3 Hz s^{-1} were applied. N_i and N_0 have similar meaning as in Figure 3; that is, the probabilities of *i*-gonal pores in (a) are referred to ΣN_i, whereas in (b), N_i is normalized to $\Sigma N_i + N_0$. The inset in (b) shows N_0 for the different deposition rates.

Representative STM images are summarized in Figure 7. Deposition with intermediate and high rates results in comparable network qualities with no statistically significant differences. Counterintuitively, extremely slow deposition (<0.01 Hz s^{-1}) results in drastically impaired network quality as already discernible in the STM images (Figure 7c,d). Consequently, the pore geometry distributions in Figure 8 show extraordinary high probabilities of pentagonal and even tetragonal pores. On the other hand, slower deposition aids in decreasing the relative amount of open pores. Slight differences were also found in the APCN, where deposition with a rate of <0.01 Hz s^{-1} leads to a value of 3.2, whereas the two higher deposition rates result in APCN values of 4.0 (0.1 Hz s^{-1}) and 4.3 (1.3 Hz s^{-1}).

To improve the network quality, fundamental insights into defect formation and the influence of kinetic reaction parameters are required. A clear experimental result is the increased number of open pores at lower polymerization temperatures, similarly observed for both hierarchical and direct polymerization. Two different reasons account for this observation: incomplete debromination and insufficient lateral mobility of the building blocks. At domain boundaries, dangling molecular lobes with a length of (0.8 ± 0.1) nm can be inferred from STM images, indicating still brominated phenyl rings (cf. Supporting Information). In this case, the polymerization can only proceed along the reactive sites, and these pores cannot be completed.

Previously, Fasel *et al.* studied the influence of surface mobility by comparing the polymerization of iodinated CHP on the (111) facets of Cu, Ag, and Au.[17] On Cu(111), branched networks were observed, the compactness was improved for Au(111), and densely packed networks were obtained on Ag(111). In accompanying MC simulations, the network morphology similarly changed from branched to compact for lower ratios of coupling to diffusion. Analogously, we observe more compact networks for higher surface temperature, both in our experiments and Monte Carlo simulations (*vide infra*). By analogy with the results for different surfaces, we conclude that the limited lateral monomer mobility at lower temperatures and the presence of still not fully activated (*i.e.*, debrominated sites) account for the large amount of open pores. In this respect, higher surface temperatures should be advantageous. On the other hand, higher temperatures similarly enhance the probabilities for irregular pores, as statistically deduced for both direct and hierarchical polymerization.

In the following, kinetic arguments are used to rationalize irregular pore formation. The enhanced amount of pentagonal pores with increasing temperature may be explained by postulating a highly strained and thus high-energy transition state.[11] During the course of polymerization, each pentamer unit can become either a regular hexagonal pore by adding one more monomer in a bimolecular reaction or an irregular pentagonal pore through an unimolecular macro-ring closure. The bimolecular reaction rate is proportional to the concentration of activated, that is, dehalogenated monomers which increases with deposition rate. On the other hand, the unimolecular ring closing requires only thermal energy to overcome the barrier. Accordingly, the reaction rate increases with temperature. As a result, the network morphology is determined by the competition between bimolecular and unimolecular reactions, in full agreement with the experimental findings, where either higher surface temperatures or extremely slow deposition promote the formation of irregular pores.

Direct *versus* Hierarchical Polymerization. Comparison of directly and hierarchically polymerized networks reveals certain morphological differences. Hierarchical polymerization leads to small densely packed domains that are frequently interconnected by molecular chains and single-pore-wide strings, while comparable motifs have never been observed for direct polymerization. Differences regarding irregular pore formation are more subtle: Direct polymerization exhibits a steeper temperature gradient for the probability of pentagonal pores than hierarchical polymerization. Irregular pores are also crucial for hierarchical polymerization but are less prone to thermal activation. Furthermore, at 185 °C, the APCN for hierarchical polymerization at 185 °C of 1.9 is even higher than 1.1 for direct polymerization. For higher surface temperatures, instead, the APCN of hierarchical polymerization does not exceed 3.0, occupying an intermediate position between 4.3 for direct polymerization at 250 °C and 2.6 for 375 °C.

MC Simulations. To comprehend the influence of reaction parameters, MC simulations were conducted. Principally, these simulations cannot account for irregular pores but are suitable to understand the evolution of network morphologies for different building block structures and reaction parameters. Comparative MC simulations were performed for direct *versus* hierarchical polymerization with monomers and dimers as molecular building blocks, respectively. The coupling probability p was used as a free parameter. It is defined as $p = (\nu_{coupl}/(\nu_{coupl} + \nu_{diff}))$ with ν_{coupl} and ν_{diff} as coupling and diffusion rates. Accordingly, low p values correspond to high surface mobility of building blocks in relation to the incorporation probability into the network. On the contrary, high p values close to unity indicate immediate and irreversible bond formation. In a similar study of a six-fold monomer, different p values were assigned to different surface materials.[17] By comparison with experimental results, the lowest p value was matched with Ag(111). It was previously suggested that both coupling and diffusion are associated with energy barriers E_{coupl} and E_{diff}.[17,27] Based on the assumption $E_{coupl} < E_{diff}$, lower p values correspond to higher surface temperatures with enhanced surface mobility of building blocks. However, a direct conversion of p values into surface temperatures is not easily possible since this would require detailed knowledge of the temperature dependence of ν_{coupl} and ν_{diff}, that is, exponential prefactors and activation barriers when assuming an Arrhenius law.

Figure 9 summarizes MC results for BIB and TBQ with p values of 0.01, 0.1, and 1. The evaluation of the PCN is shown in the central part, and the resulting APCNs are given in the corresponding images. For both building blocks, lower p leads to more compact aggregates, whereas more branched networks were obtained for higher p. Accordingly, the APCN decreases with increasing p for BIB and TBQ, whereby higher APCNs are generally obtained for BIB. Larger APCNs were also experimentally observed for higher surface temperatures, thereby confirming the initial assumption that decreasing p corresponds to increasing surface temperatures. In this context, the experimental results exhibit a noteworthy exception for direct polymerization. The highest experimental APCN of 4.3 was obtained at 250 °C; however, for 375 °C, the experimental APCN decreases to 2.6. This observation contradicts the MC simulations, which suggest a further APCN improvement for even higher surface temperatures. This discrepancy might indicate a limiting influence of the enhanced amount of irregular pores observed at higher surface temperatures on the compactness of the domains and APCNs.

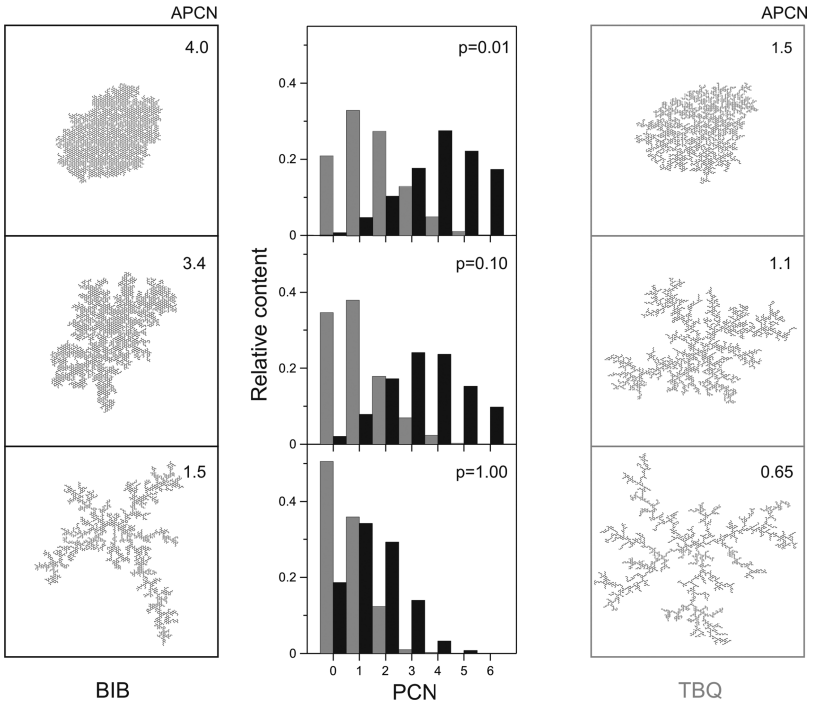

Figure 9. Summary of MC results for direct *versus* hierarchical polymerization. In the left and right columns, representative structures obtained for BIB *versus* TBQ polymerization for three different coupling probabilities *p* are shown (cf. Supporting Information for close-ups). Corresponding pore coordination number distributions for BIB (black) and TBQ (gray) derived networks are shown in the central part. The respective APCNs are indicated at the top right corners.

Isolated closed pores without any neighboring closed pore (PCN = 0) were found in both experiment and simulation for lower surface temperature and higher *p*, respectively. Yet, the MC simulations yield a significantly higher amount of isolated pores for hierarchical than for direct polymerization, whereas the experimental situation is reversed (cf. Supporting Information). This discrepancy indicates an overestimation of the stability of isolated pore configurations in MC simulations. Quantitative deviations between experiment and MC simulation might originate in inappropriate modeling of diffusion or rotation of the larger TBQ in comparison to the smaller BIB – an effect that becomes particularly evident in the direct comparison of different species. Moreover, the improved network quality for the smaller building block in the MC simulations originates in the assumption of immobile oligomers. Accordingly, growth only occurs due to addition of further monomers to the fixed seed. In the real situation, however, larger oligomers are most likely still mobile on the surface – especially at higher surface temperature – leading to polymerization mechanisms that resemble step growth.

Concerning structures and configurations, MC simulations of TBQ result in unique morphologies that are directly comparable to the experiments: 1D chains and strings of pores were frequently observed both in the experiment and MC simulations (cf. Supporting Information). Moreover, the simulations suggest different formation routes for hexagonal pores from either three, four, or six TBQ monomers (cf. Supporting Information).

CONCLUSION

The influence of different kinetic reaction parameters on the morphology and defect density of covalent networks obtained by on-surface Ullmann coupling was studied on Au(111) using an iodine- and bromine-functionalized aromatic precursor. At room temperature, iodine is selectively split off, whereas bromine dissociation requires further thermal activation. This well-documented temperature dependence of C–Br and C–I bond cleavage is confirmed by the present work and utilized for a comparative study of different polymerization protocols. Both hierarchical and direct polymerization resulted in covalent networks with open and irregular (tetragonal, pentagonal, heptagonal, and octagonal) pores as the most common defects. The effect of different reaction parameters was identified by a quantitative comparison of the network quality based on a statistical analysis of STM data.

For both polymerization protocols, similar temperature effects were observed: Lower surface temperatures result in a relatively large amount of open pores. In accord with Monte Carlo, this can be attributed to the limited lateral mobility of building blocks. Furthermore, not yet completed debromination may also play an important role at lower temperatures. Increased surface temperatures do not only reduce the amount of open pores but also improve the compactness of the

networks as expressed in increased APCNs. On the other hand, irregular pores dominate at higher surface temperature, an effect that is more pronounced for direct polymerization. Interestingly, direct polymerization with very slow deposition rates (*i.e.* deposition over the course of several hours) slightly improves the APCN but results in the highest observed amounts of pentagonal and tetragonal pores. Both experimentally observed dependencies can consistently be explained by a kinetic competition between bimolecular reactions that result in regular hexagonal pores and unimolecular ring-closing reactions that result in irregular tetragonal or pentagonal pores. The unimolecular reaction is associated with a notable activation barrier, hence becomes favored at higher temperatures, whereas the bimolecular reaction rate depends on the availability of monomers and increases with deposition rate. These on-surface polymerization results bear a noteworthy analogy to solution chemistry: in a kinetic competition between polymerization and cyclization, the latter becomes favored under high-dilution conditions,[32] which corresponds to low deposition rates in on-surface chemistry.

On the basis of the statistical analysis, we propose mutually exclusive structure optimization criteria for covalent networks: lower surface temperatures reduce irregular pore formation; however, by the same token, limited diffusivity and incomplete debromination at lower temperatures result in dendritic morphologies and more open pores. Consequently, surfaces that promote high diffusivity of surface-stabilized radicals would be the better choice. Yet, this implementation of on-surface Ullmann coupling still requires the catalytic activity of surfaces for initiating the polymerization by carbon−halogen bond cleavage, which limits this approach to metals. In this respect, Au(111) might still be the best compromise in terms of sufficient catalytic activity and low diffusion barriers for activated monomers.

The differences between on-surface Ullmann coupling of BIB and TBQ (*i.e.*, direct and hierarchical polymerization) are surprisingly small. Even though both protocols result in networks with relatively high defect densities, the preceding dimerization step in hierarchical polymerization aids in reducing the amount of irregular pores, especially at higher surface temperatures. It is particularly instructive to compare the present results to the hierarchical polymerization of *trans*-Br_2I_2 tetraphenyl porphyrin.[31] In direct comparison to the fully brominated analogue, Grill *et al.* infer an overall improvement of the structural quality with notably enhanced domain size and postulate this to be a direct consequence of low defect densities. Indeed, in the present case, high amounts of irregular pores coincide with low APCN, possibly indicating a correlation between defect densities and domain sizes. An important difference between the two systems is that in the first step *trans*-Br_2I_2 tetraphenyl porphyrin can already polymerize into 1D chains that are subsequently interlinked into 2D networks. Thereby, a templating molecular zipper effect of the 1D chain, which is however absent in the present system, appears to be a key ingredient for improving the structural quality. This molecular zipper effect was also observed in a metal-directed polymerization by Lin *et al.* on Au(111), where the presence of extrinsic copper adatoms was found to induce a templating effect that leads to structural improvement.[33] In summary, hierarchical polymerization based on the different activation barriers of deiodination and debromination on gold surfaces is a reliable approach to either initiate and study different polymerization pathways or to sequentially build up more complex structures in on-surface Ullmann coupling.

MATERIALS AND METHODS

STM Experiments. All experiments were carried out under UHV conditions with a base pressure of 2×10^{-10} mbar. Au(111) single-crystal surfaces were prepared by cycles of Ar^+ ion-sputtering and subsequent annealing at 500 °C. Synthesis details of BIB are provided in the Supporting Information. BIB was deposited by sublimation from a home-built Knudsen cell with crucible temperatures of 126 to 168 °C, yielding deposition rates of 0.3×10^{-3} 0.2 monolayer min^{-1}. To precisely control the deposition rates and to verify their long-term stability, a Knudsen cell with integrated QCMB was used.[34] During deposition, the surface was held either at room temperature or at elevated temperatures of 185, 250, and 375 °C. After room temperature deposition, the polymerization was activated by subsequent thermal annealing with different rates and final temperatures. All samples were characterized *in situ* by means of a home-built scanning tunneling microscope operating at room temperature.

STM images were statistically analyzed by pore counting. Thereby, the pore geometry and the number of adjacent pores were taken into account. Open pores were only considered when they were more than halfway closed. For each parameter set, the analysis encompassed at least 100 pores, typically 200 pores. Uncertainty values are given as the square root of counts. Macroscopically different sample areas were compared to reduce the influence of sample inhomogeneities.

MC Simulations. A modified version of the conventional diffusion-limited aggregation (DLA) algorithm with fractal growth on a seed was used.[35,36] The simulations were performed on a 1000×1000 rhombic segment of a triangular lattice of equivalent adsorption sites. The monomers for direct (BIB) and hierarchical (TBQ) polymerization were modeled as rigid flat three-fold-star- and dumbbell-shaped building blocks comprising four and eight identical segments, respectively, each of which occupied one lattice site (cf. Supporting Information). Initially, an immobile seed molecule of BIB or TBQ was placed at the center of the lattice. An annular launch zone centered at the seed was defined, where subsequent molecules start surface diffusion. During the simulation, this launch zone was adjusted to account for the increasing size of the aggregate. It was delimited by two concentric circles with an inner radius of $r + 20$ lattice spacings and an outer radius of $r + 40$ lattice spacings (r corresponds to the distance between seed and the segment which is furthest from the center). Deposition was implemented

by releasing molecules from random positions within the launch zone. Surface diffusion was simulated by randomly performing a series of short-distance jumps into one of the six equivalent directions. A special feature of the proposed model, which distinguishes it from conventional DLA growth models, is the requirement of appropriate molecular orientation. Bond formation is only possible when the respective arms of the reacting molecules are collinearly aligned (cf. Supporting Information). To account for this effect, surface diffusion was accompanied by a random in-plane rotation of the building blocks by a multiple of 60°. For the tripod, the rotation axis lies in the central segment, while for the dumbbell, one of the two core segments was chosen at random (cf. Supporting Information). Accordingly, in each simulation step, either diffusion or rotation was performed with equal probability. Once diffusing molecules encounter the growing network and their relative positions and orientations are suitable for bond formation, a uniformly distributed random number $\in(0,1)$ was generated. If the number was smaller than the preset coupling probability $0 \leq p \leq 1$, the molecule was irreversibly incorporated into the cluster; otherwise, the molecule was allowed to diffuse and rotate further. Diffusing molecules that crossed the outer boundary of the launch zone were discarded and replaced by new molecule as described previously. The simulations were run until either the number of steps exceeded 10^4 or the network had reached a mass of 8000 molecular segments, corresponding to 2000 BIB and 1000 TBQ, and statistically analyzed.

Conflict of Interest: The authors declare no competing financial interest.

Acknowledgment. Financial support by the Nanosystems-Initiative Munich Cluster of Excellence and the DFG is gratefully acknowledged (DFG LA1842/4-1).

Supporting Information Available: BIB synthesis; additional statistical data: pore geometry distribution for different heating rates; pore coordination number distributions; DFT calculations; additional STM data; additional MC results. This material is available free of charge *via* the Internet at http://pubs.acs.org.

REFERENCES AND NOTES

1. Gourdon, A. On-Surface Covalent Coupling in Ultrahigh Vacuum. *Angew. Chem., Int. Ed.* **2008**, *47*, 6950–6953.
2. Martin-Gago, J. A. Polycyclic Aromatics On-Surface Molecular Engineering. *Nat. Chem.* **2011**, *3*, 11–12.
3. Perepichka, D. F.; Rosei, F. Extending Polymer Conjugation into the Second Dimension. *Science* **2009**, *323*, 216–217.
4. Colson, J. W.; Dichtel, W. R. Rationally Synthesized Two-Dimensional Polymers. *Nat. Chem.* **2013**, *5*, 453–465.
5. Gutzler, R.; Perepichka, D. F. π-Electron Conjugation in Two Dimensions. *J. Am. Chem. Soc.* **2013**, *135*, 16585–16594.
6. Zwaneveld, N. A. A.; Pawlak, R.; Abel, M.; Catalin, D.; Gigmes, D.; Bertin, D.; Porte, L. Organized Formation of 2D Extended Covalent Organic Frameworks at Surfaces. *J. Am. Chem. Soc.* **2008**, *130*, 6678–6679.
7. Ourdjini, O.; Pawlak, R.; Abel, M.; Clair, S.; Chen, L.; Bergeon, N.; Sassi, M.; Oison, V.; Debierre, J.-M.; Coratger, R.; *et al.* Substrate-Mediated Ordering and Defect Analysis of a Surface Covalent Organic Framework. *Phys. Rev. B* **2011**, *84*, 125421.
8. Zhang, Y.-Q.; Kepčija, N.; Kleinschrodt, M.; Diller, K.; Fischer, S.; Papageorgiou, A. C.; Allegretti, F.; Björk, J.; Klyatskaya, S.; Klappenberger, F.; *et al.* Homo-coupling of Terminal Alkynes on a Noble Metal Surface. *Nat. Commun.* **2012**, *3*, 1286.
9. Gao, H.-Y.; Franke, J.-H.; Wagner, H.; Zhong, D.; Held, P.-A.; Studer, A.; Fuchs, H. Effect of Metal Surfaces in On-Surface Glaser Coupling. *J. Phys. Chem. C* **2013**, *117*, 18595–18602.
10. Eichhorn, J.; Heckl, W. M.; Lackinger, M. On-Surface Polymerization of 1,4-Diethynylbenzene on Cu(111). *Chem. Commun.* **2013**, *49*, 2900–2902.
11. Schlögl, S.; Heckl, W. M.; Lackinger, M. On-Surface Radical Addition of Triply Iodinated Monomers on Au(111) — The Influence of Monomer Size and Thermal Post-processing. *Surf. Sci.* **2012**, *606*, 999–1004.
12. Grill, L.; Dyer, M.; Lafferentz, L.; Persson, M.; Peters, M. V.; Hecht, S. Nano-architectures by Covalent Assembly of Molecular Building Blocks. *Nat. Nanotechnol.* **2007**, *2*, 687–691.
13. Fan, Q.; Wang, C.; Han, Y.; Zhu, J.; Kuttner, J.; Hilt, G.; Gottfried, J. M. Surface-Assisted Formation, Assembly, and Dynamics of Planar Organometallic Macrocycles and Zigzag Shaped Polymer Chains with C—Cu—C Bonds. *ACS Nano* **2013**, *8*, 709–718.
14. Walch, H.; Gutzler, R.; Sirtl, T.; Eder, G.; Lackinger, M. Material- and Orientation-Dependent Reactivity for Heterogeneously Catalyzed Carbon—Bromine Bond Homolysis. *J. Phys. Chem. C* **2010**, *114*, 12604–12609.
15. Cai, J.; Ruffieux, P.; Jaafar, R.; Bieri, M.; Braun, T.; Blankenburg, S.; Muoth, M.; Seitsonen, A. P.; Saleh, M.; Feng, X.; *et al.* Atomically Precise Bottom-Up Fabrication of Graphene Nanoribbons. *Nature* **2010**, *466*, 470–473.
16. Blunt, M. O.; Russell, J. C.; Champness, N. R.; Beton, P. H. Templating Molecular Adsorption Using a Covalent Organic Framework. *Chem. Commun.* **2010**, *46*, 7157–7159.
17. Bieri, M.; Nguyen, M.-T.; Gröning, O.; Cai, J.; Treier, M.; Aït-Mansour, K.; Ruffieux, P.; Pignedoli, C. A.; Passerone, D.; Kastler, M.; *et al.* Two-Dimensional Polymer Formation on Surfaces: Insight into the Roles of Precursor Mobility and Reactivity. *J. Am. Chem. Soc.* **2010**, *132*, 16669–16676.
18. Lipton-Duffin, J. A.; Ivasenko, O.; Perepichka, D. F.; Rosei, F. Synthesis of Polyphenylene Molecular Wires by Surface-Confined Polymerization. *Small* **2009**, *5*, 592–597.
19. Eder, G.; Smith, E. F.; Cebula, I.; Heckl, W. M.; Beton, P. H.; Lackinger, M. Solution Preparation of Two-Dimensional Covalently Linked Networks by Polymerization of 1,3,5-Tri(4-iodophenyl)benzene on Au(111). *ACS Nano* **2013**, *7*, 3014–3021.
20. Russell, J. C.; Blunt, M. O.; Garfitt, J. M.; Scurr, D. J.; Alexander, M.; Champness, N. R.; Beton, P. H. Dimerization of Tri(4-bromophenyl)benzene by Aryl—Aryl Coupling from Solution on a Gold Surface. *J. Am. Chem. Soc.* **2011**, *133*, 4220–4223.
21. Lipton-Duffin, J. A.; Miwa, J. A.; Kondratenko, M.; Cicoira, F.; Sumpter, B. G.; Meunier, V.; Perepichka, D. F.; Rosei, F. Step-by-Step Growth of Epitaxially Aligned Polythiophene by Surface-Confined Reaction. *Proc. Natl. Acad. Sci. U.S.A.* **2010**, *107*, 11200–11204.
22. Wang, W.; Shi, X.; Wang, S.; Van Hove, M. A.; Lin, N. Single-Molecule Resolution of an Organometallic Intermediate in a Surface-Supported Ullmann Coupling Reaction. *J. Am. Chem. Soc.* **2011**, *133*, 13264–13267.
23. Gutzler, R.; Walch, H.; Eder, G.; Kloft, S.; Heckl, W. M.; Lackinger, M. Surface Mediated Synthesis of 2D Covalent Organic Frameworks: 1,3,5-Tris(4-bromophenyl)benzene on Graphite(001), Cu(111), and Ag(110). *Chem. Commun.* **2009**, 4456–4458.
24. Schlögl, S.; Sirtl, T.; Eichhorn, J.; Heckl, W. M.; Lackinger, M. Synthesis of Two-Dimensional Phenylene-Boroxine Networks through *In Vacuo* Condensation and On-Surface Radical Addition. *Chem. Commun.* **2011**, *47*, 12355–12357.
25. Gutzler, R.; Cardenas, L.; Lipton-Duffin, J.; El Garah, M.; Dinca, L. E.; Szakacs, C. E.; Fu, C.; Gallagher, M.; Vondracek, M.; Rybachuk, M.; *et al.* Ullmann-Type Coupling of Brominated Tetrathienoanthracene on Copper and Silver. *Nanoscale* **2014**, *6*, 2660–2668.
26. Eichhorn, J.; Strunskus, T.; Rastgoo-Lahrood, A.; Samanta, D.; Schmittel, M.; Lackinger, M. On-Surface Ullmann Polymerization *via* Intermediate Organometallic Networks on Ag(111). *Chem. Commun.* **2014**, *50*, 7680–7682.
27. Björk, J.; Hanke, F.; Stafström, S. Mechanisms of Halogen-Based Covalent Self-Assembly on Metal Surfaces. *J. Am. Chem. Soc.* **2013**, *135*, 5768–5775.
28. Di Giovannantonio, M.; El Garah, M.; Lipton-Duffin, J.; Meunier, V.; Cardenas, L.; Fagot Revurat, Y.; Cossaro, A.; Verdini, A.; Perepichka, D. F.; Rosei, F.; *et al.* Insight into Organometallic Intermediate and Its Evolution to Covalent

Bonding in Surface-Confined Ullmann Polymerization. *ACS Nano* **2013**, *7*, 8190–8198.
29. Bieri, M.; Blankenburg, S.; Kivala, M.; Pignedoli, C. A.; Ruffieux, P.; Müllen, K.; Fasel, R. Surface-Supported 2D Heterotriangulene Polymers. *Chem. Commun.* **2011**, *47*, 10239–10241.
30. Saywell, A.; Greń, W.; Franc, G.; Gourdon, A.; Bouju, X.; Grill, L. Manipulating the Conformation of Single Organometallic Chains on Au(111). *J. Phys. Chem. C* **2013**, *118*, 1719–1728.
31. Lafferentz, L.; Eberhardt, V.; Dri, C.; Africh, C.; Comelli, G.; Esch, F.; Hecht, S.; Grill, L. Controlling On-Surface Polymerization by Hierarchical and Substrate-Directed Growth. *Nat. Chem.* **2012**, *4*, 215–220.
32. Ziegler, K. Uber Ringschluß-Reaktionen. *Ber. Deutsch. Chem. Ges.* **1934**, *67*, A139–A149.
33. Lin, T.; Shang, X. S.; Adisoejoso, J.; Liu, P. N.; Lin, N. Steering On-Surface Polymerization with Metal-Directed Template. *J. Am. Chem. Soc.* **2013**, *135*, 3576–3582.
34. Gutzler, R.; Heckl, W. M.; Lackinger, M. Combination of a Knudsen Effusion Cell with a Quartz Crystal Microbalance: *In Situ* Measurement of Molecular Evaporation Rates with a Fully Functional Deposition Source. *Rev. Sci. Instrum.* **2010**, *81*, 015108.
35. Barabási, A.-L.; Stanley, H. E. *Fractal Concepts in Surface Growth*; Cambridge University Press: Cambridge, 1995.
36. Avnir, D. *The Fractal Approach to Heterogeneous Chemistry*; John Wiley and Sons Inc.: New York, 1989.